Control of inner cells' proportion by asymmetric divisions and ensuing resilience of cloned rabbit embryos

Authors

Dimitri Fabrèges[1]†

Nathalie Daniel[2]

Véronique Duranthon[2]

Nadine Peyriéras[1]*

Affiliations

[1] BioEmergences Laboratory, CNRS USR 3695, 91190 Gif-sur-Yvette, France.

[2] UMR BDR, INRA, ENVA, Université Paris Saclay, 78350, Jouy en Josas, France.

* Corresponding authors: Nadine Peyriéras (nadine.peyrieras@cnrs.fr)

† Present address: Developmental Biology Unit, European Molecular Biology Laboratory (EMBL), Heidelberg, Germany.

Summary statement

A unique quantitative approach based on cell lineage complete reconstruction, that unveils an unknown mechanism of size control in cell populations of rabbit blastocysts, wild types or clones.

Summary

Mammalian embryo cloning by nuclear transfer has a low success rate. This is hypothesized to correlate with a high variability of early developmental steps segregating outer cells, fated to extraembryonic tissues, from inner cells, giving rise to the embryo proper. Exploring the cell lineage of wild-type embryos (WT) and clones, imaged *in toto* until hatching, highlights the respective contributions of cell proliferation, death and asymmetric divisions to phenotypic variability. Preferential cell death of inner cells in clones, probably pertaining to the epigenetic plasticity of the transferred nucleus, is identified as a major difference with consequences on the inner cell proportion. In WT and clones, similar patterns of outer cell asymmetric divisions are shown to be essential to the robust inner cell proportion observed in WT. Asymmetric inner cell division, not described in mice, is identified as a regulator of the inner cell proportion, likely to give rise to resilient clones.

Keywords

rabbit preimplantation development, somatic cell nuclear transfer, digital specimens, spatial cell segregation, asymmetrical divisions, cell death, in silico experimentation, 3D+time 2-photon imaging

List of Symbols and Abbreviations

WT: wild-type; NT: nuclear transferred; SCNT: Somatic Cell Nuclear Transfer; h.p.f.: hours post-fertilization; h.p.a.: hours post-activation; n.a.: normalized age.

Introduction

Variability goes along with the possibility of adapting to changing environments (Darwin, 1859). Consistently, wild-type populations are intrinsically variable (Raj and van Oudenaarden, 2008). The production of inbred strains as achieved in laboratory conditions in mice aimed at minimizing genotypic and phenotypic variability (Beck et al., 2000). Animal cloning by somatic cell nuclear transfer (SCNT) has been developed to go a step further in keeping desired traits and produce clones in different mammalian species (Hochedlinger and Jaenisch, 2002; Inoue et al., 2005; Wakayama et al., 1999). However, the cloning efficiency is low (Hochedlinger and Jaenisch, 2003; Yang et al., 2007) and much effort has been devoted to improving its success rate. Following SCNT, embryonic development eventually resumes and leads to a normal organism. However, whether the developmental path of clones falls within the normal range of embryonic variability in terms of cell identity, proliferation, division orientation and death, remains to be explored.

Quantitative studies investigating multiscale phenotypic variability in bacteria (Elowitz et al., 2002; So et al., 2011; Taniguchi et al., 2010), yeasts (Blake et al., 2003; Carey et al., 2013) and metazoans (Boettiger and Levine, 2009; Ohnishi et al., 2014; Wernet et al., 2006) have been published. However, the quantification of variability at the level of genetic expression and cell behavior in mammalian embryos relies mainly on the observation of fixed specimens. The current challenge is to achieve the *in vivo* and *in toto* multiscale observation of developing embryos, in order to perform a systematic quantitative analysis of phenotypic traits and model the multiscale variability. The cellular scale of organization is expected to integrate variation at the subcellular level (e.g., thermal agitation and stochastic gene expression) as well as cues from the macroscopic organization (e.g., mechanical constraints)

and from environmental conditions. Long-term *in toto* imaging of preimplantation mammalian embryos has been recently reported in mice (Strnad et al., 2015), with a difficult tradeoff between photodamage (Squirrell et al., 1999), spatial and temporal resolution required to achieve the full automated reconstruction of cell lineage and cell shapes as done in other species (Amat et al., 2014; Faure et al., 2016; Fernandez et al., 2010). Mammalian embryos develop from fertilization to the blastocyst stage in a few days, segregating two cell populations distinguished by their position and presumptive fate. Outer cells form an epithelial layer fated to form extra-embryonic tissues. Inner cells form a cluster in the blastocoel cavity giving rise to the embryo proper. Although the same organization is observed in almost all mammalian species, possible differences in underlying cell behaviors is largely unknown. Additionally, the possibility to extrapolate our knowledge to human requires investigating biological diversity. In this context, the rabbit *Oryctolagus cuniculus* has been described as more similar to human than the mouse, for certain phenotypic traits (Duranthon et al., 2012; Okamoto et al., 2011; Piliszek et al., 2017).

We investigated the variability of cell dynamics in normal and cloned rabbit embryos from the entire cell lineage reconstructed from 2-photon microscopy images throughout preimplantation stages. The quantitative comparison of cell death, cell proliferation and division orientation in inner and outer cell populations highlights defects and possible resilience in clones. The asymmetric division of inner cells, not yet described in the mouse, are shown to have the appropriate patterns to regulate the size of the inner cell population observed at the time of hatching. This putative mechanism would not, however, be able to compensate for the most severe inner cell death cases. The epigenetic state of donor cells and their ability to give rise to embryonic cells adapted to the cellular environment of both the inner and outer domains of the developing blastula is likely to be at stake.

Results

Digital specimens were obtained from 3D+time imaging of three WT embryos (wt1-3) and two clones (nt1,2), nuclear-stained by injection at the one-cell stage of synthetic mRNA encoding H2B-EGFP and developing from the 32-cell stage until hatching (Fig. 1, Movies S1,2). RNA concentration and imaging conditions were optimized and did not affect embryo survival and cell growth (Table S1 and Fig. S1). Clones were obtained by SCNT using cumulus cells taken from the oocyte donor female. Fully curated cell lineages were submitted to an automated analysis of spatiotemporal characteristic features (Fig. 1F-J, see methods).

The cell number over time (Fig. 1L) showed different paces from one embryo to another, impairing further inter-individual comparison. We therefore normalized the embryo developmental speed. Temporal rescaling based on morphogenetic events led to the best fit in terms of cell number and embryonic volume evolution (Fig. S2 and Note S1). Fertilization (for WT) or activation (for clones) and the first blastocoel collapse were taken as fixed points, 0 and 1 respectively, for the temporal rescaling of the different specimens and the calculation of a normalized age (n.a.) (Fig. 1M, Table S2 and Movie S3). The comparison between the different specimens is thereafter limited to the common period from 0.768 to 1.073 n.a. Cell growth in clones appeared slower than that of WT (12% and 17% slower for nt1 and nt2 respectively). In addition to growing slower than the wild types, the two clones differed from each other, while the three WT embryos looked quite similar in terms of growth rate. However, as viable clones have been shown to form kits of normal size (Challah-Jacques et al., 2003), we assumed that differences in growth rate could be compensated at later stages and we expected to find severer abnormalities to explain the very low success rate of rabbit cloning.

Because variations in single cell positions from one embryo to another prevented the identification of individual cells across specimens, the inner and outer cell populations appeared to be the relevant level of organization to further compare embryonic cell dynamics. While the average inner and outer cell numbers were similar between WT and clones, the latter had a higher inner cell number standard deviation (Fig. 1N,O). Despite the small number of embryos supporting this observation, we hypothesized that the variability of the inner cell number may correlate with the low survival rate described in SCNT embryos, since an insufficient number of inner cells leading to a smaller inner-to-total cell ratio would compromise embryonic development, as described in mice (Morris et al., 2012).
Looking for an explanation of the variability of the inner cell number appeared to be relevant for further comparison of WT and clones. This variability was not explained by differences in their cell division rate (Fig. 2 and Fig. S3), but we noted a highly variable number of inner cells at the onset of the observation (Fig. S4), indicating that the overall inner cell number would thereafter be highly sensitive to cell death and/or asymmetric divisions. A division is identified as asymmetric when daughter cells are found in different compartments (inner and outer) (see methods). Cell death was clearly identified in 3D+time imaging data (Movie S4). It was confirmed by TUNEL assay that the proportion of cell death in inner or outer cell populations was similar in injected, non-injected and imaged embryos (Fig.S1). Cell death

obviously had dramatic consequences on the size of already small populations. We observed this type of incidence for nt1 and wt3 during the first 0.1 n.a. (30% and 39% inner cell death for populations of 3 and 9 cells respectively: Fig. S4G,I,J,L). Overall, we did not observe any characteristic temporal distribution pattern of cell death to discriminate between wild-type embryos and clones. The spatial distribution of cell death, however, indicated a marked bias for inner cell death in clones, with a normalized death ratio of 2.32 (s.d. = 0.03) in inner cells compared to 0.63 (s.d. = 0.26) in outer cells, while cell death was independent of cell type in wild-type embryos (normalized death ratio of 1.03 for inner cells with s.d. = 0.90 and 1.06 for outer cells with s.d. = 0.31) (Fig. 3A). Inner cell death bias thus appeared as a major difference between clones and WT embryos. Surprisingly, this bias did not prevent clones from reaching a proportion of inner cells similar to that of wild types (Fig. 3B). Asymmetric cell division was the only possible process remaining to explain how the proportion of inner cells, initially much lower on average in clones compared to wild-type embryos, increased then plateaued before the first collapse (Fig. 3C-H, Fig. S5 and Table S3) at a value close to the average observed in wild types and possibly corresponding to a critical threshold (Morris et al., 2012). Asymmetric divisions were identified for both outer cells and inner cells (Movies S5,6). The distribution of asymmetric divisions in outer cells feeding the inner cell population was quite similar in clones and WT. Consequently, this could not explain the increase in the proportion of inner cells observed in clones, rising from half of the value observed in WT at the onset of the observation sequence to the same value by 0.93 n.a. The best explanation of the clones' recovery seemed to come from the distribution of the asymmetric divisions of inner cells. Although asymmetric divisions of inner cells were observed in both WT and clones, very few were observed in the latter, and only at late stages. Asymmetric divisions of inner cells, never yet described in mice, were found preferentially for cells close to the outer layer (Fig. 3I), suggesting positional and or mechanical cues. We propose that the asymmetric division of inner cells functions as an ultimate regulation process to balance the proportion of inner cells, in both WT and clones.

The putative contribution of inner cells' asymmetric divisions to regulating the size of the inner cell population is supported by the transformation of asymmetric divisions into symmetric ones *in silico* and the simulation of the corresponding cell lineages (Fig. 4 and Fig. S6). It should be noted that by the onset of the imaging sequence, the inner cell population has already been built by earlier outer cells' asymmetric divisions, so that the simulation does not impair the evolution of cell populations that relies on symmetric divisions. The variability of the outer cell population, estimated by the standard deviation over the mean cell number,

remains low in both wild types and clones in experimental conditions. The variability remains low upon simulation with the transformation of asymmetric divisions into symmetric ones either for outer cells (Fig. 4B,E) or for inner cells (Fig. 4C,F). Thus, the size of the outer cell population is robust regarding the contribution of asymmetric divisions. Conversely, the size of the inner cell population in wild types becomes early on (0.85 n.a.) highly variable upon transformation of the observed outer cells' asymmetric divisions into symmetric ones. We interpret that in the latter case, the simulation reveals the intrinsic variability of the inner cell number related to variable cell death. This variability is consistent with the inner cell population variability observed in clones both in experimental conditions and upon simulation. We hypothesize that after the bulk of outer cells asymmetric divisions that built the inner cell population and depending on the extent of cell death, adjusting the size of the inner cell population and the inner to total cell ratio is based on inner cells' asymmetric divisions. Consistently, the evolution of the inner to total cell ratio in simulated lineages (Fig. S6), similar in wild types and clones upon transformation of outer cells' asymmetric divisions, fits with delayed and scarce inner cells' asymmetric divisions in clones. Our interpretation is that the normal regulation of the inner cell population size leads to a tradeoff between robust embryonic development and the space of variability that is potentially available for resilience.

Discussion

The cell lineage phenomenology of rabbit preimplantation embryogenesis lays the basis for comparisons and extrapolation to human. Similar studies in other species are, however, yet to be produced. Available live imaging data in mice only encompasses the first 6 divisions (Strnad et al., 2015). Our data focused on later stages starting by the fifth generation. Rabbit development was impaired when imaged earlier, possibly correlating with the timing of their zygotic activation. Our study was limited by embryo survival to mRNA injection and long-term imaging (3 days). Nuclear transfer further compromising the success rate. In addition, only 20% of embryos imaged until hatching led to an exploitable full cell lineage, due to various imaging artefacts.

Comparing individuals first required a temporal rescaling. Taking the first collapse as a landmark led to similar patterns of asymmetric divisions in outer cells, validating our choice and also indicating some internal constraints in the relative timing of specific morphogenetic events. Our time-lapse imaging data suggest a wave of asymmetric divisions in rabbit

embryos between the 32- and 64-cell stages. The presence of inner cells at the onset of our imaging sequences indicates that earlier waves may have happened. In the mouse, at least two waves have been described by the 8- to 16-cell stage and the 16- to 32-cell stage (Johnson, 1981; Johnson and McConnell, 2004; Morris et al., 2012; Sutherland et al., 1990; Wennekamp and Hiiragi, 2012). The occurrence of a third wave by the 32- to 64-cell stage has been mentioned (Morris et al., 2010). In any case, this last wave of asymmetric division of outer cells is essential to forming the inner cell mass in a robust manner, as highlighted by our *in silico* transformation of the asymmetric divisions of outer cells into symmetric ones. A more striking difference between the mouse and the rabbit may lie in the occurrence of asymmetric inner cell divisions. We hypothesize that the ratio of asymmetric inner cell divisions is regulated to reach and maintain an optimal value of the proportion of inner cells. The hypothesis of such a regulatory scenario is supported by the observation of clones where an initial low proportion of inner cells correlates with a low ratio of asymmetric inner cell divisions. In this context and given the importance of this ratio for proper development, asymmetric inner cell divisions should be found in the mouse as well.

The low survival rate observed in SNCT rabbit embryos should be consistent with major differences between viable and non-viable specimens in quantitative parameters including cell proliferation and cell death. Our observations suggest that inner cell death is the major issue. The higher cell death rate observed in the inner cell population of clones could lead to a higher variability of their inner cell population compared to wild types sufficient to explain their low survival rate (Hochedlinger and Jaenisch, 2003; Yang et al., 2007). These observations pertain to the epigenetic state of the transferred nucleus and the transfer protocol that brings the membrane and cytoplasm of the donor cell to the egg. The epigenetic state of the transferred nucleus may confer limited potency to the blastomeres, leading to a better survival rate in the trophectoderm than in the inner cell mass. The adaptive capacity of the donor nucleus to fit both the inside and outside environments is probably the major issue. It should be noted that IPS cells or ES cells that might be expected to solve this issue are not currently available in the rabbit. More generally, animal cloning by somatic cell nuclear transfer is a powerful strategy for assessing cell plasticity and its potential for variation and chance for selection through cell-environment interaction.

Materials and Methods

Animals and embryo culture. Experiments were performed in accordance with the International Guiding Principles for Biomedical Research involving animals, as promulgated by the Society for the Study of Reproduction and the European Convention on Animal Experimentation. Researchers working with the animals possessed a license delivered by the French veterinary services.

New Zealand White female rabbits (*Oryctolagus cuniculus*) were superovulated as described in Ref. (Henrion et al., 1997) and mated with normal males (giving rise to wild-type embryos) or vasectomized males (for clones). One-cell stage embryos were flushed from oviducts with PBS at 19 hours postcoitum (h.p.c.). Synthetic mRNA at a concentration of 75 ng/µL in water was injected at the one cell stage at 38.5°C in M199 medium with 10% FBS, 0.5% penicillin/streptomycin and 20 mM HEPES (bM199-FBS). Embryos were kept at 38.5°C under 5% CO_2 in bM199-FBS without HEPES (M199-FCS) with phenol-red in a humid incubator until the morula stage. Embryos were then transported for imaging in a drop of bM199-FBS in a capillary. The temperature was maintained at 38°C during the transportation to the imaging location, where embryos were kept in M199-FBS.

Assessing cell death. Chromatin fragmentation and cell behavior including nucleus abnormal displacement, interrupted mitosis and disruption of the nuclear envelope were used to annotate cell death in 3D+time imaging data. A TUNEL assay (ref. 12156792910, Sigma-Aldrich, USA) was used to assess cell death in embryos cultured until 69 hpc, 73 hpc and 93 hpc and fixed with phosphate buffer saline 0.1M pH 7.5 (PBS, ref. 189112-04, Invitrogen, USA) and 2.5% paraformaldehyde for 1 hour at 4ºC. Embryos were rinsed in PBS 1X and permeabilized in PBS 1X, 0.5% Triton X-100 for 1 hour at room temperature. After 1 hour incubation in the TUNEL reaction mix at 38ºC, embryos were rinsed in SSC 2X, then PBS 1X. Nucleus counterstain was achieved with 4µM Hoechst-33342 (ref. H1399, Invitrogen, USA) in PBS for 15 minutes. Embryos were rinsed in PBS and imaged immediately with a Zeiss confocal LSM-780. Hoechst-33342 and TMR-Red were excited at 405 nm and 543 nm. TMR-red signal was used to annotate apoptotic cells.

Cloning by nuclear transfer. Rabbit oocytes without cumulus cells were enucleated as described in Ref. (Challah-Jacques et al., 2003). Cumulus cells were introduced into the subzonal space of enucleated oocytes. Cell-oocyte pairs were electrostimulated to induce

fusion. One hour later, fused embryos were activated by a second set of electric pulses followed by one hour of incubation with 5 µg/mL cycloheximide and 2 mM 6-dimethylaminopyridine in M199-FBS. Clones were then cultured as done for wild-type embryos.

Embryo mounting and imaging. Imaging was performed with Leica DM5000 and DM6000 upright microscopes SP5 MLSM, equipped with an Olympus 20/0.95NA W dipping lens objective or a Leica 20/1NA W dipping lens objective. For wt1 and wt2, the field size was 455.68×455.68 µm in x and y, and 174.24 µm in z, with a voxel size of $0.89 \times 0.89 \times 1.76$ µm. For wt3 and nt1, the field size was 529.41×529.41 µm in x and y, and 241.27 µm in z, with a voxel size of $1.034 \times 1.034 \times 1.049$ µm. For nt2, the field size was 412.67×412.67 µm in x and y, and 222.36 µm in z, with a voxel size of $0.806 \times 0.806 \times 0.797$ µm. Volumes were acquired every 15 minutes. 2-photon excitation at 980 nm was performed with a pulsed laser beam (Ti-Sapphire femtosecond oscillator Mai Tai HP, Newport Spectra physics). Laser power was automatically modulated with a motorized half-wave plate, a polarized cube and real-time feedback to maintain a relatively constant signal-to-noise ratio. Emission signal was filtered with a 680 nm short-pass filter (Semrock, USA) to remove infrared reflection and a 525/50 nm band-pass filter (Semrock, USA). Photon detection was done with hybrid detectors (Hamamatsu Photonics K.K., Japan, for Leica, Germany). OKO-lab H101 system was used for temperature control. OKO-lab DGT-CO2 system was used to control CO_2 concentration. Raw data movies were made with Fiji (Schindelin et al., 2012). Raw data are available online at http://bioemergences.eu/fabreges-et-al

Digital reconstruction. Reconstruction were performed on single specimen. A manual region of interest (ROI) was made to enclose each specimen. Signal intensity outside the ROI was set to zero masking other specimens in the field of view. Embryos were reconstructed with the BioEmergences Workflow as described in Ref. (Faure et al., 2016). Nuclear centers were detected with the Difference of Gaussians algorithm, parameters were manually selected every 25 timesteps to best fit the raw data and interpolated over the whole imaging sequence. Tracking was done with the Simulated Annealing algorithm. Cell lineages were manually curated with the software Mov-IT (Faure et al., 2016) either until hatching (wt1, wt3, nt1 and nt2) or earlier when the fluorescent signal was too weak (wt2). Cells were annotated as inner cells or outer cells based on the nucleus position at the last time step. Annotations were then propagated backwards along the cell lineage and mitoses were

checked for their type (symmetric or asymmetric). Raw and reconstructed data are available online at http://bioemergences.eu/fabreges-et-al.

Temporal Rescaling. The time of fertilization of wild-type embryos was estimated as 8 hours post-coitum as measured previously (Pincus and Enzmann, 1935). The activation time for clones was set at the time of the second electric pulses. Fertilization and activation times were used to define the first fixed point for rescaling (time 0.0 n.a.). The overall embryo volume was estimated with the surface enveloping the outermost nuclei (convex hull), calculated using the R geometry package (Habel et al., 2015). The first decrease of more than 10% in the hull volume from one time-step to the next was taken as the first blastocoel collapse (80.7 h.p.f, 77.7 h.p.f, 86.8 h.p.f, 92.3 h.p.a. and 96.0 h.p.a. for wt1, wt2, wt3, nt1 and nt2 respectively) and used as the second fixed point for rescaling (time 1.0 n.a.).

In silico **experiment.** Considering the cell identity only, asymmetric divisions were transformed into symmetric divisions *in silico*. The cell lineages were modified making daughters' identity matches the mother's identity. This operation was performed for all inner cells or for all outer cells depending on the condition. Cell position or trajectory was not modified and only the resulting cell identity was compared between conditions.

Analysis of the reconstructed data. CSV files containing information for cell position, temporal links and annotations (validation, inner, outer) were constructed and analyzed with custom R scripts. Annotation of cell divisions (symmetry or asymmetry) was determined based on the identity of mother and daughter cells prior to their next mitosis. If daughter cells did not divide by the end of the imaging sequence, their identity at the last time step was used. When measurements were analyzed from pools of embryos (WT versus clones), they were resampled over time to obtain the same number of time points. The finest temporal resolution was preserved and data were interpolated linearly if necessary.

R scripts. Custom R scripts were written to perform specific analyses with Base libraries (Team, 2015) and the geometry package (Habel et al., 2015). Graphs and figures were generated using ggplot2 (Wickham, 2009) and rgl (Adler and Murdoch, 2016) packages for R.

Competing interests

No competing interests declared

Author contributions

Conceptualization, D.F. and N.P.; Methodology, D.F. and N.P.; Formal Analysis, D.F.; Investigation, D.F. and N.D.; Resources, V.D. and N.P.; Data Curation, D.F.; Writing – Original Draft, D.F. and N.P.; Writing – Review & Editing, D.F., N.P., V.D. and N.D.; Visualization, D.F.; Supervision, N.P. and V.D.; Project Administration, N.P.; Funding Acquisition, N.P. and V.D.

Data availability

Datasets are available on the BioEmergences website, http://bioemergences.eu/fabreges-et-al/.

Correspondence and material requests should be addressed to Nadine Peyriéras: nadine.peyrieras@cnrs.fr.

References

Adler, D. and Murdoch, D. (2016). rgl: 3D Visualization Using OpenGL.

Amat, F., Lemon, W., Mossing, D. P., McDole, K., Wan, Y., Branson, K., Myers, E. W. and Keller, P. J. (2014). Fast, accurate reconstruction of cell lineages from large-scale fluorescence microscopy data. *Nat. Methods* **11**, 951–8.

Beck, J. A., Lloyd, S., Hafezparast, M., Lennon-Pierce, M., Eppig, J. T., Festing, M. F. W. and Fisher, E. M. C. (2000). Genealogies of mouse inbred strains. *Nat. Genet.* **24**, 23–25.

Blake, W. J., KAErn, M., Cantor, C. R. and Collins, J. J. (2003). Noise in eukaryotic gene expression. *Nature* **422**, 633–637.

Boettiger, A. N. and Levine, M. (2009). Synchronous and stochastic patterns of gene activation in the Drosophila embryo. *Science* **325**, 471–473.

Carey, L. B., van Dijk, D., Sloot, P. M. A., Kaandorp, J. A. and Segal, E. (2013). Promoter Sequence Determines the Relationship between Expression Level and Noise. *PLoS Biol.* **11**,.

Challah-Jacques, M., Chesné, P. and Renard, J. P. (2003). Production of Cloned Rabbits by Somatic Nuclear Transfer. *Cloning Stem Cells* **5**, 295–299.

Darwin, C. (1859). *On the origins of species by means of natural selection*. John Murray.

Duranthon, V., Beaujean, N., Brunner, M., Odening, K. E., Santos, A. N., Kacskovics, I., Hiripi, L., Weinstein, E. J. and Bosze, Z. (2012). On the emerging role of rabbit as human disease model and the instrumental role of novel transgenic tools. *Transgenic Res.* **21**, 699–713.

Elowitz, M. B., Levine, A. J., Siggia, E. D. and Swain, P. S. (2002). Stochastic gene expression in a single cell. *Science* **297**, 1183–6.

Faure, E., Savy, T., Rizzi, B., Melani, C., Stašová, O., Fabrèges, D., Špir, R., Hammons, M., Čúnderlík, R., Recher, G., et al. (2016). A workflow to process 3D+time microscopy images of developing organisms and reconstruct their cell lineage. *Nat. Commun.* **7**, 8674.

Fernandez, R., Das, P., Mirabet, V., Moscardi, E., Traas, J., Verdeil, J.-L., Malandain,

G. and Godin, C. (2010). Imaging plant growth in 4D: robust tissue reconstruction and lineaging at cell resolution. *Nat. Methods* **7**, 547–553.

Habel, K., Grasman, R., Gramacy, R. B., Stahel, A. and Sterratt, D. C. (2015). geometry: Mesh Generation and Surface Tesselation.

Henrion, G., Brunet, A., Renard, J. P. and Duranthon, V. (1997). Identification of maternal transcripts that progressively disappear during the cleavage period of rabbit embryos. *Mol. Reprod. Dev.* **47**, 353–362.

Hochedlinger, K. and Jaenisch, R. (2002). Monoclonal mice generated by nuclear transfer from mature B and T donor cells. *Nature* **415**, 1035–1038.

Hochedlinger, K. and Jaenisch, R. (2003). Nuclear Transplantation, Embryonic Stem Cells, and the Potential for Cell Therapy. *N. Engl. J. Med.* **349**, 275–286.

Inoue, K., Wakao, H., Ogonuki, N., Miki, H., Seino, K. I., Nambu-Wakao, R., Noda, S., Miyoshi, H., Koseki, H., Taniguchi, M., et al. (2005). Generation of cloned mice by direct nuclear transfer from natural killer T cells. *Curr. Biol.* **15**, 1114–1118.

Johnson, M. H. (1981). The foundation of two distinct cell lineages within the mouse morula. *Cell* **24**, 71–80.

Johnson, M. H. and McConnell, J. M. L. (2004). Lineage allocation and cell polarity during mouse embryogenesis. *Semin. Cell Dev. Biol.* **15**, 583–597.

Morris, S. a, Teo, R. T. Y., Li, H., Robson, P., Glover, D. M. and Zernicka-Goetz, M. (2010). Origin and formation of the first two distinct cell types of the inner cell mass in the mouse embryo. *Proc. Natl. Acad. Sci. U. S. A.* **107**, 6364–9.

Morris, S. A., Guo, Y. and Zernicka-Goetz, M. (2012). Developmental plasticity is bound by pluripotency and the fgf and wnt signaling pathways. *Cell Rep.* **2**, 756–65.

Ohnishi, Y., Huber, W., Tsumura, A., Kang, M., Xenopoulos, P., Kurimoto, K., Oleś, A. K., Araúzo-Bravo, M. J., Saitou, M., Hadjantonakis, A.-K., et al. (2014). Cell-to-cell expression variability followed by signal reinforcement progressively segregates early mouse lineages. *Nat. Cell Biol.* **16**, 27–37.

Okamoto, I., Patrat, C., Thépot, D., Peynot, N., Fauque, P., Daniel, N., Diabangouaya, P., Wolf, J.-P., Renard, J.-P., Duranthon, V., et al. (2011). Eutherian mammals use diverse strategies to initiate X-chromosome inactivation during development. *Nature*

472, 370–374.

Piliszek, A., Madeja, Z. E. and Plusa, B. (2017). Suppression of ERK signalling abolishes primitive endoderm formation but does not promote pluripotency in rabbit embryo. *Development* dev.156406.

Pincus, G. and Enzmann, E. V (1935). The Comparative Behavior of Mammalian Eggs in vivo and in vitro. *J. Exp. Med.* **62**, 665–675.

Raj, A. and van Oudenaarden, A. (2008). Nature, Nurture, or Chance: Stochastic Gene Expression and Its Consequences. *Cell* **135**, 216–226.

Schindelin, J., Arganda-Carreras, I., Frise, E., Kaynig, V., Longair, M., Pietzsch, T., Preibisch, S., Rueden, C., Saalfeld, S., Schmid, B., et al. (2012). Fiji: an open-source platform for biological-image analysis. *Nat. Methods* **9**, 676–682.

So, L.-H., Ghosh, A., Zong, C., Sepúlveda, L. a, Segev, R. and Golding, I. (2011). General properties of transcriptional time series in Escherichia coli. *Nat. Genet.* **43**, 554–560.

Squirrell, J. M., Wokosin, D. L., White, J. G. and Bavister, B. D. (1999). Long-term two-photon fluorescence imaging of mammalian embryos without compromising viability. *Nat. Biotechnol.* **17**, 763–7.

Strnad, P., Gunther, S., Reichmann, J., Krzic, U., Balazs, B., de Medeiros, G., Norlin, N., Hiiragi, T., Hufnagel, L. and Ellenberg, J. (2015). Inverted light-sheet microscope for imaging mouse pre-implantation development. *Nat. Methods* **13**, 1–7.

Sutherland, a. E., Speed, T. P. and Calarco, P. G. (1990). Inner cell allocation in the mouse morula: The role of oriented division during fourth cleavage. *Dev. Biol.* **137**, 13–25.

Taniguchi, Y., Choi, P. J., Li, G.-W., Chen, H., Babu, M., Hearn, J., Emili, A. and Xie, X. S. (2010). Quantifying E. coli Proteome and Transcriptome with Single-Molecule Sensitivity in Single Cells. *Science* **329**, 533–538.

Team, R. C. (2015). *R: A Language and Environment for Statistical Computing*. Vienna, Austria: R Foundation for Statistical Computing.

Wakayama, T., Rodriguez, I., Perry, A. C., Yanagimachi, R. and Mombaerts, P. (1999). Mice cloned from embryonic stem cells. *Proc. Natl. Acad. Sci. U. S. A.* **96**, 14984–14989.

Wennekamp, S. and Hiiragi, T. (2012). Stochastic processes in the development of pluripotency in vivo. *Biotechnol. J.* **7**, 737–744.

Wernet, M. F., Mazzoni, E. O., Celik, A., Duncan, D. M., Duncan, I. and Desplan, C. (2006). Stochastic spineless expression creates the retinal mosaic for colour vision. *Nature* **440**, 174–180.

Wickham, H. (2009). *ggplot2: Elegant Graphics for Data Analysis*. New York (N.Y.): Springer-Verlag.

Yang, X., Smith, S. L., Tian, X. C., Lewin, H. A., Renard, J.-P. and Wakayama, T. (2007). Nuclear reprogramming of cloned embryos and its implications for therapeutic cloning. *Nat. Genet.* **39**, 295–302.

Figures
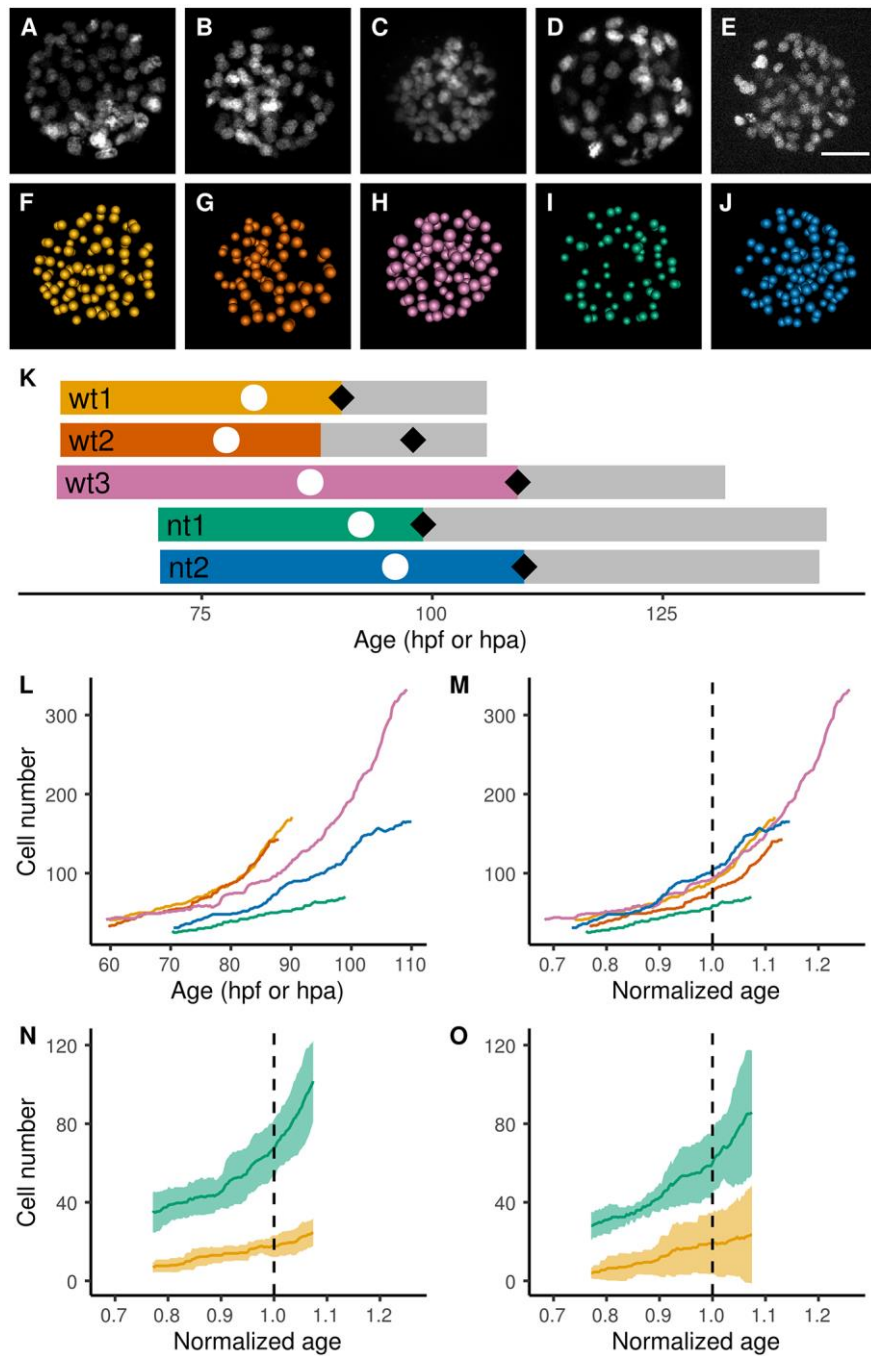
Fig. 1. Reconstruction of digital rabbit specimens from 3D+time imaging of labeled nuclei. (**A**-**M**) wt1 (orange), wt2 (vermillon), wt3 (reddish purple), nt1 (bluish green) and nt2 (blue). (**A**-**E**) Z-projection of 3D volumes, 15 minutes before the first blastocoel collapse. (**F**-**J**) Z-projection of reconstructed embryos at the same timestep. Each approximate nucleus

center is represented by a sphere. (**A-J**) Scale bar: 50µm. (**K,L**) Age based on fertilization time (h.p.f., WT embryos) and activation time (h.p.a., clones). (**K**) Time line of the imaging sequences. The cell lineage validation and curation is limited to the colored part. White disc: first collapse. Black diamond: hatching. (**L**) Cell number over time without temporal rescaling. (**M-O**) Cell number over time with temporal rescaling based on the fertilization or activation time and first blastocoel collapse. Dashed line: first blastocoel collapse. (**N**) Average number of inner cells (orange line) and outer cells (bluish green line) in WT embryos. Standard deviation is shown as a semi-transparent area. (**O**) Average cell number in clones. Color code as in **N**.
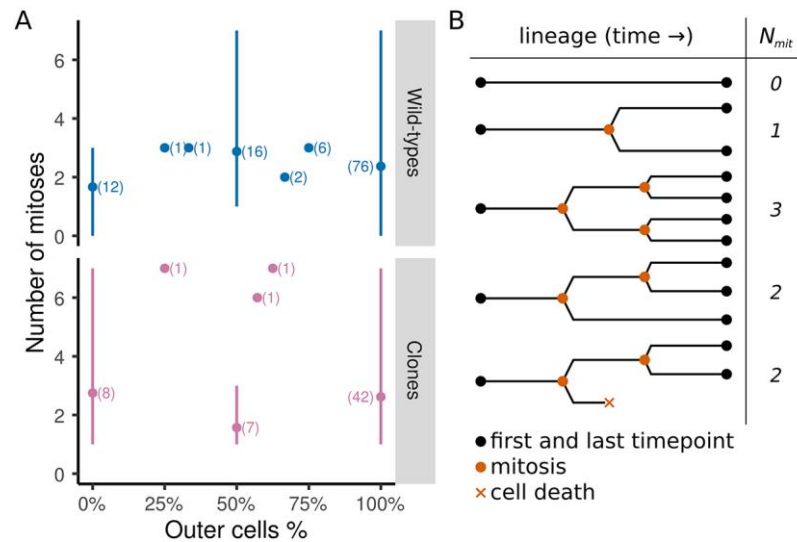
Fig. 2. Number of mitoses and cell identity along the cell lineage. (**A**) Average number of mitoses as a function of cells' identity in each cell clone: each cell at the onset of the observation window gives rise to a cell clone with a proportion of inner and outer cells depending on mitosis type and cell death. The percentage of cells of each type is plotted against the corresponding number of mitoses (solid lines to indicate the minimum and maximum number of mitoses and dot to indicate the average number of mitoses). (**Top**) WT embryos (n=114 cells). (**Bottom**) Clones (n=60 cells). (**B**) Typical binary trees are schematized with different patterns of cell division and death (temporal progression from left to right). N_{mit}: number of mitoses in the cell clone.
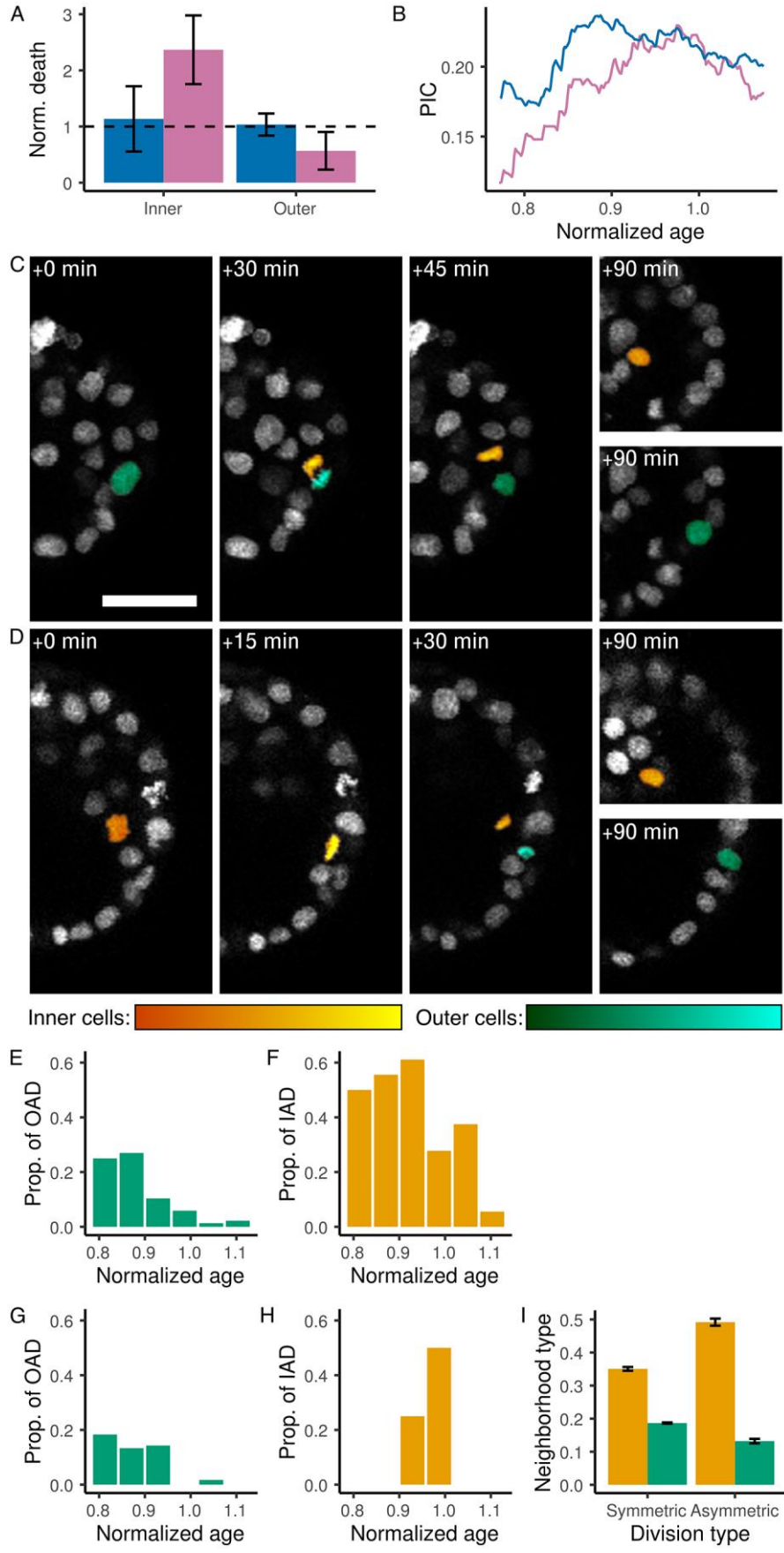
Inner cells: Outer cells:

Fig. 3. Contribution of cell death and asymmetric divisions to the proportion of inner cells. (**A**) Normalized death ratio (Norm. death) for inner and outer cells in WT embryos (blue) and clones (reddish purple). Standard error in black solid line. Dashed line indicates the normalized death ratio if cell death and cell type were not correlated. (**B,E-I**) Time in n.a. (**B**) Average proportion of inner cells (PIC) in WT (blue) and clones (reddish purple). (**C**) Example of an outer cell asymmetric division in wt3 (by 91.75 h.p.f. ≈ 1.058 n.a.). Scale bar: 50 µm. (**D**) Example of an inner cell asymmetric division in wt3 (by 101.5 h.p.f. ≈ 1.171 n.a.). Scale bar as in (**C**). (**E-H**) Bin size 0.05 n.a. ≈ 4.3 hours. Outer cells in bluish green. Inner cells in orange. (**E,G**) Proportion of asymmetric divisions in outer cells (OAD). (**F,H**) Proportion of asymmetric divisions in inner cells (IAD). (**E,F**) WT embryos. (**G,H**) Clones. (**I**) Average proportion of cells of the other type in the close neighborhood of dividing cells whether symmetrically (left plots) or asymmetrically (right plots). Standard error in black solid line.
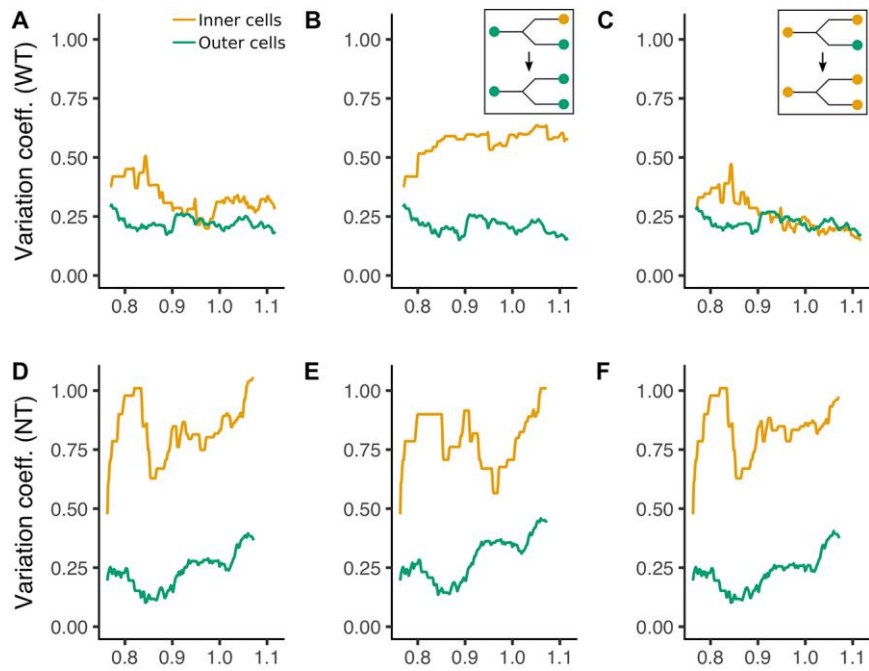
Fig. 4. Impact of the transformation of asymmetric divisions into symmetric ones on the variability of inner and outer cell populations. (**A**-**F**) Variation coefficient as a function of time in n.a. (**A-C**) in WT and (**D-F**) in clones, for inner cells (orange) and outer cells (bluish green). (**A,D**) Normal conditions. (**B,E**) Outer cell asymmetric divisions transformed into symmetric ones schematized in inset. (**C,F**) Inner cell asymmetric divisions transformed into symmetric ones schematized in inset.
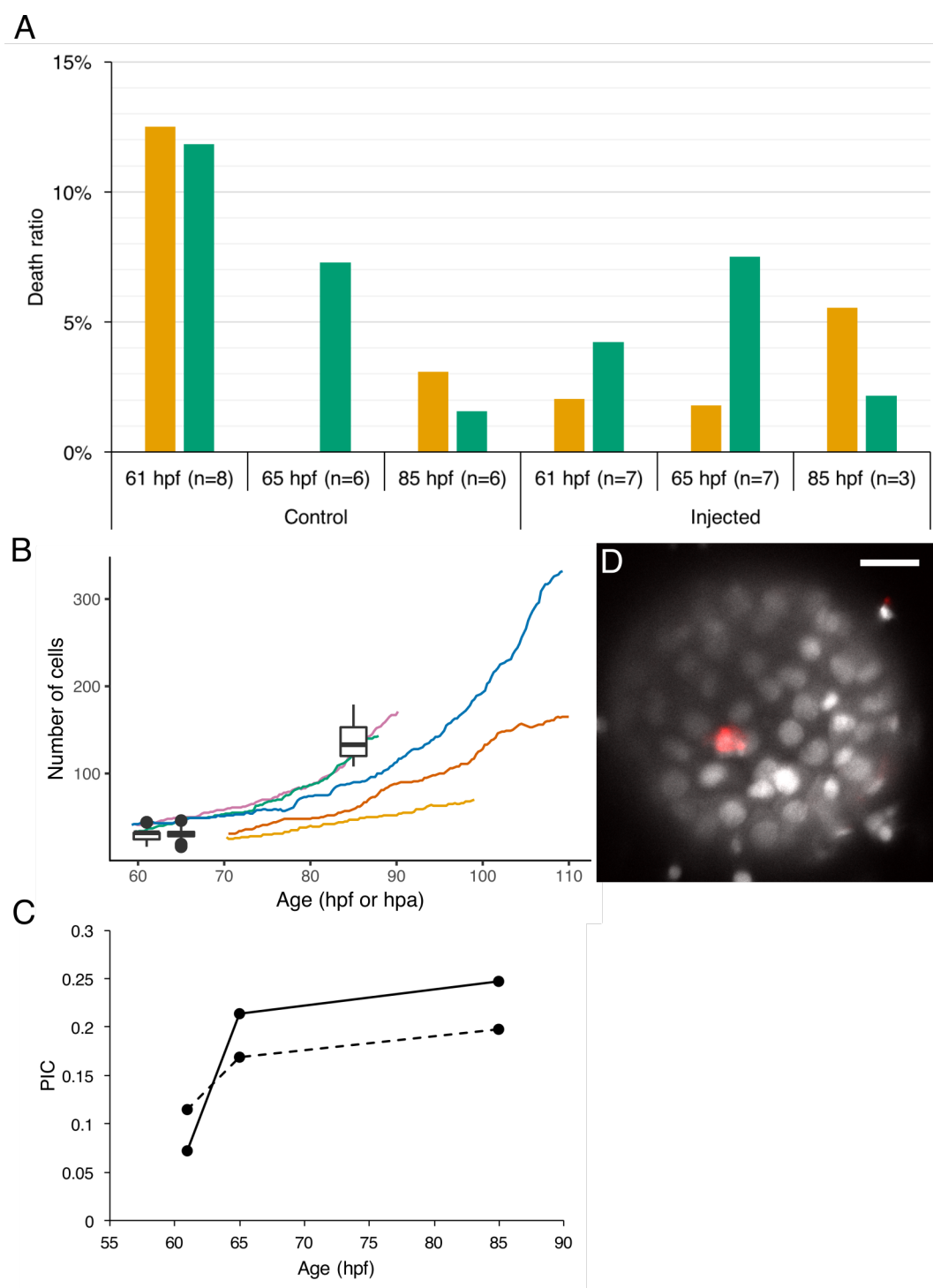
Fig. S1. Impact of RNA injection and 3D+time imaging on cell death and cell growth. (A) Proportion of TUNEL positive cells at 61 hpf, 65 hpf and 85 hpf in control and RNA-injected embryos, for inner cell (orange) and outer cell populations (bluish green). (B) Total cell number in embryos fixed at 61 hpf, 65 hpf and 85 hpf (n-values as in A) to be compared with the growth curves of embryos wt1-3 and nt1-2 (color code as in Fig. 1) shown without temporal rescaling. (C) Proportion of inner cells (PIC) in wild-type embryos fixed at 61 hpf, 65 hpf and 85 hpf (n-values as in A). Solid line: non-injected embryos. Dashed line: H2B-EGFP mRNA injected embryos. The difference in the PIC between injected and non-injected embryos is not significant (Mann-Whitney U-test, p>0.05). (D) Sum Z projection 10 μm thick from a fixed non-injected embryo (85 hpf) with stained nuclei (Hoechst in gray) and TUNEL positive cells (in red). Scale bar: 25 μm.
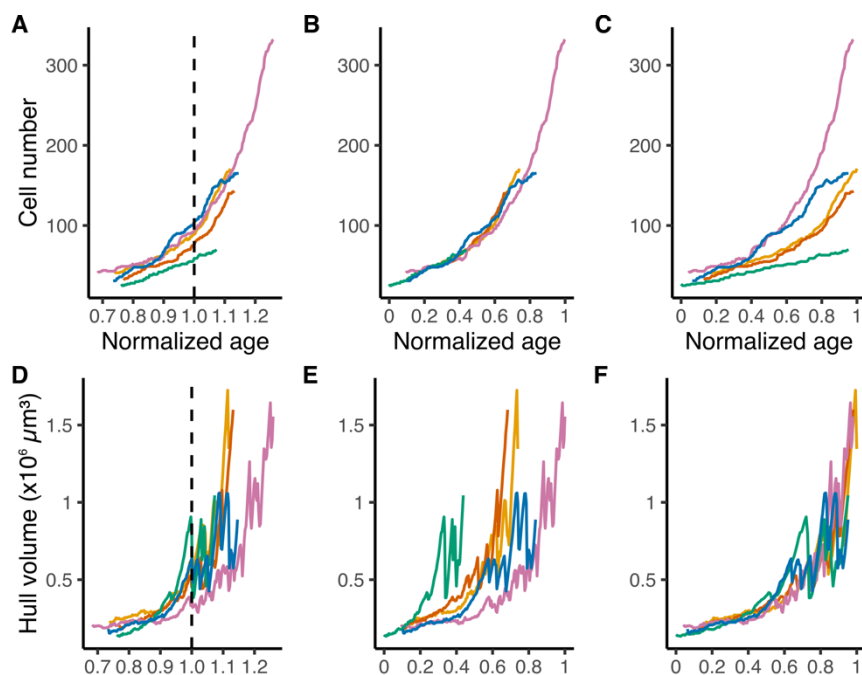
Fig. S2. Temporal rescaling. (**A-C**) Cell number over time. (**D-F**) Volume of the external envelope containing all the detected nuclei (embryo convex hull) over time. (**A,D**) Rescaling method based on morphogenetic events, i.e., fertilization or activation and first collapse. (**B,E**) Rescaling method based on the best exponential fit of cell number. (**C,F**) Rescaling method based on the best exponential fit of convex hull volume. Color code as in Fig. 1.
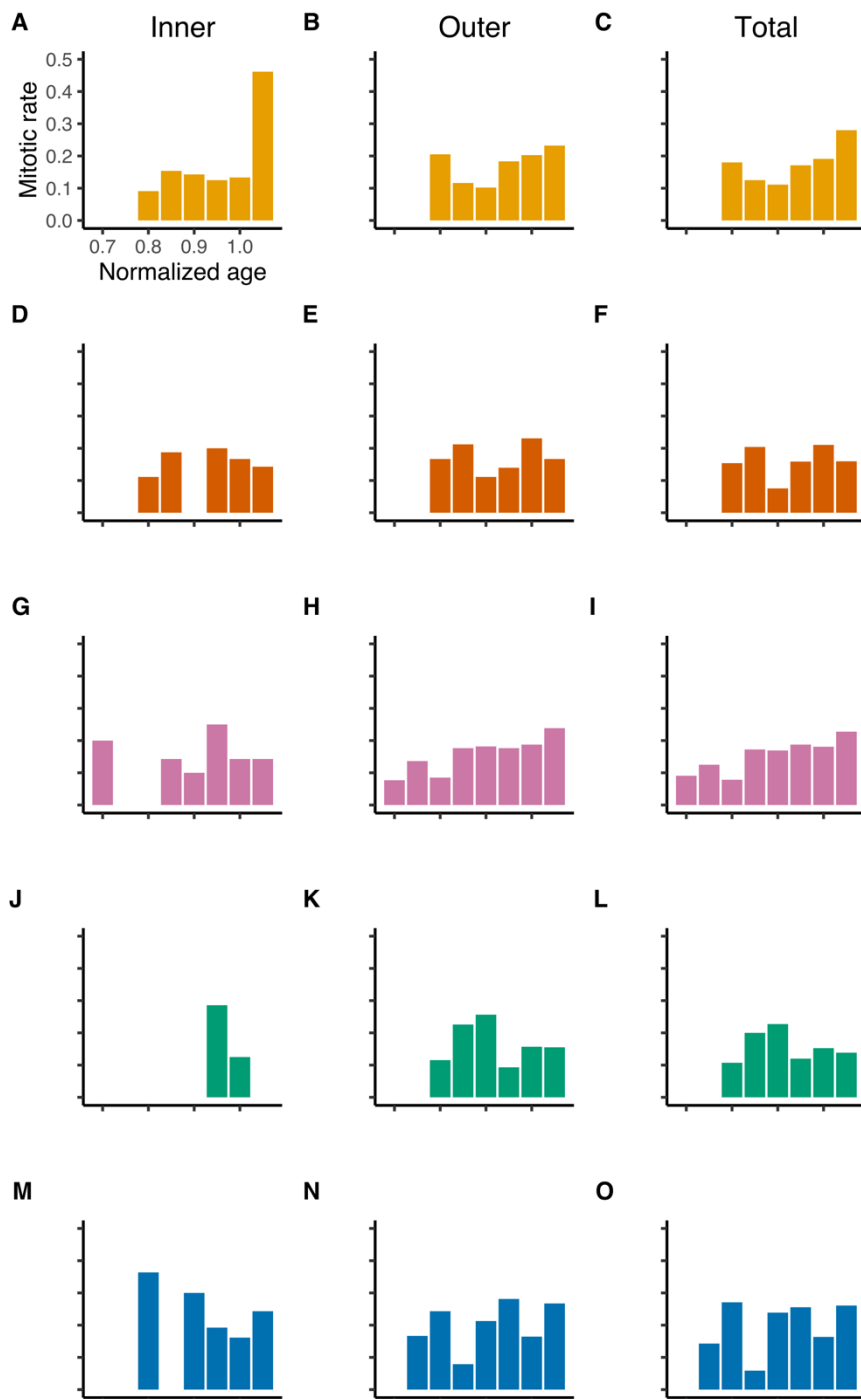
Fig. S3. Cell proliferation rate in wild-type embryos and clones over time (in n.a.). Profiles displayed for the five embryos wt1-3 and nt1,2 corresponding to rows 1 to 5 respectively. Color code as in Fig. 1. Bin size 0.05 n.a. ≈ 4.3 hours. (**First column**) Inner cell population. (**Second column**) Outer cell population. (**Third column**) All cells.
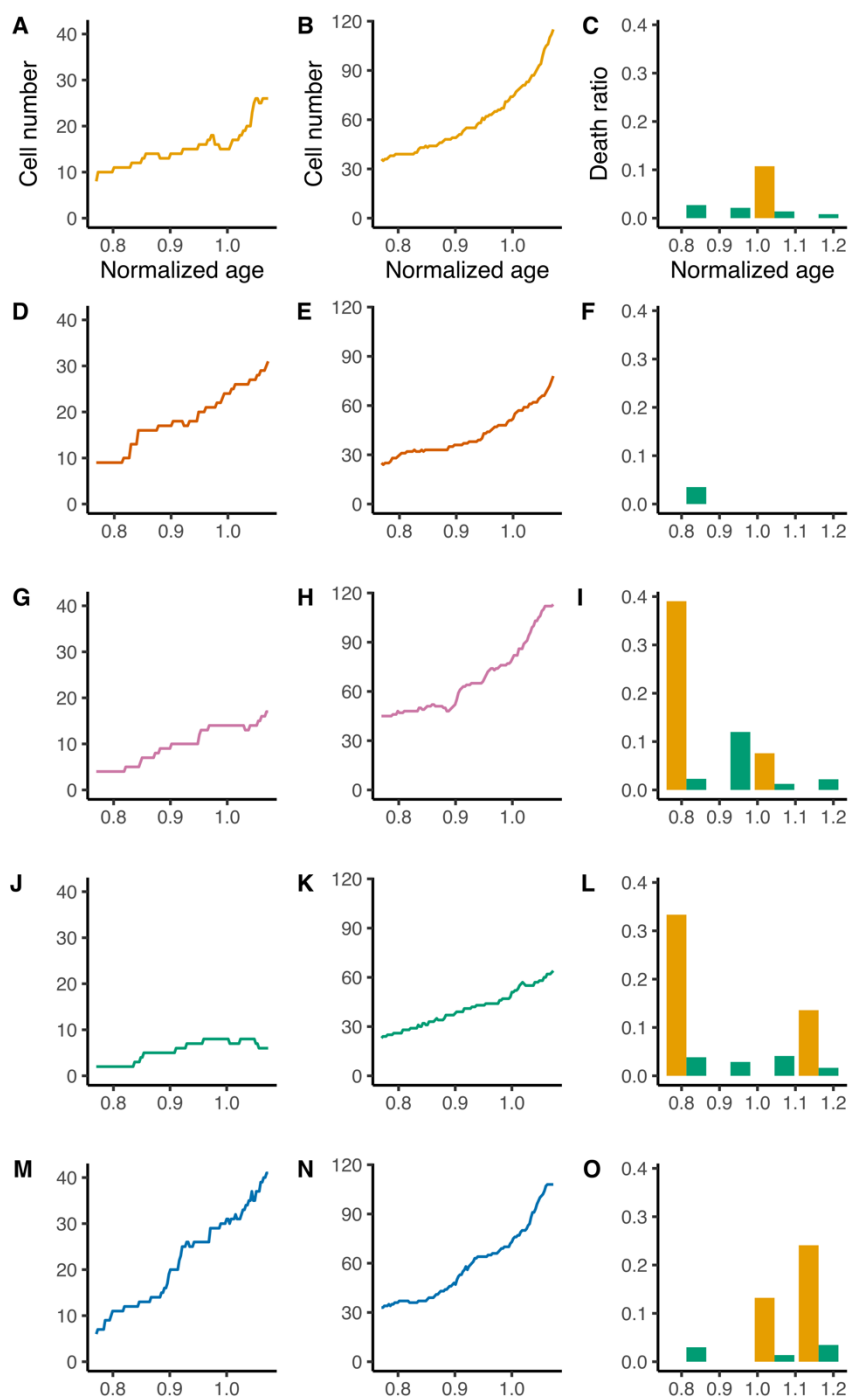
Fig. S4. Cell number and cell death rate along the cell lineage as a function of time (in n.a.). Profiles displayed for the five embryos wt1-3 and nt1,2 corresponding to rows 1 to 5 respectively. Color code as in Fig. 1. (**First column**) Inner cell number over time. (**Second column**) Outer cell number over time. (**Third column**) Cell death rate of inner cells (orange) and outer cells (bluish green) over time, expressed as the proportion of cells dying during a given time period (bin size 0.1 n.a. ≈ 8.6 hours).
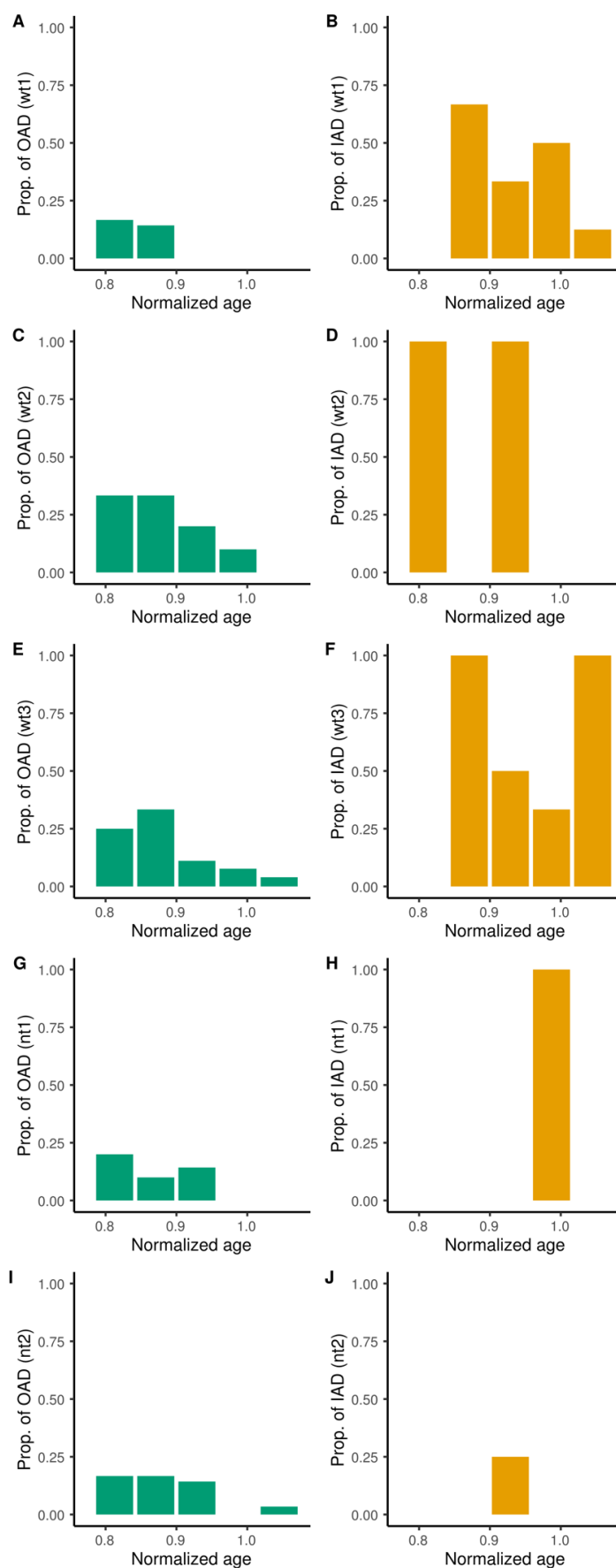
Fig. S5. Proportion of asymmetric divisions along the cell lineage as a function of time (in n.a.). Profiles displayed for the five embryos wt1-3 and nt1,2 corresponding to rows 1 to 5 respectively. Bin size 0.05 n.a. ≈ 4.3 hours. (**First column**) Proportion of outer asymmetric divisions (OAD). (**Second column**) Proportion of inner asymmetric divisions (IAD).
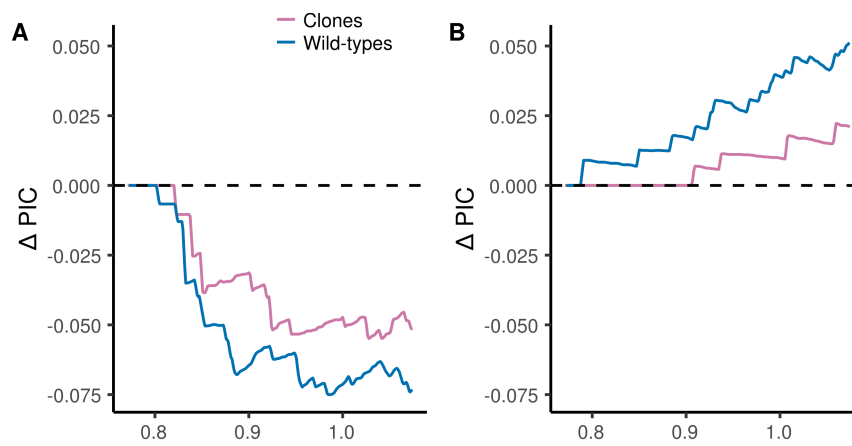
Fig. S6. Impact of the transformation of asymmetric divisions into symmetric ones on the proportion of inner cells over time (in n.a.). (A-B) Difference in the proportion of inner cells in WT (blue) and clones (reddish purple) as a function of time (in n.a.), dashed line for null difference. (**A**) Outer cell asymmetric divisions transformed into symmetric ones. (**B**) Inner cell asymmetric divisions transformed into symmetric ones.

RNA concentration	10 ng/µL each	25 ng/µL each	75 ng/µL each
Non-injected	96% (n=25)		
H2B-mCherry + EGFP-RAS	83% (n=6)	71% (n=7)	25% (n=8)
H2B-EGFP	-	-	85% (n=20)

Table S1. Survival rate of blastocysts either non-injected, or upon injection of different RNA combinations and concentrations.

n.a.[1] (a.u.)	wt & nt[2] (h.p.f/a.)	wt[3] (h.p.f.)	wt1 (h.p.f.)	wt2 (h.p.f.)	wt3 (h.p.f.)	nt[4] (h.p.a.)	nt1 (h.p.a.)	nt2 (h.p.a.)
0.65	**56h20**	**53h05**	52h25	50h30	56h25	**61h10**	59h60	62h25
0.70	**60h40**	**57h10**	56h30	54h20	60h45	**65h55**	64h35	67h10
0.75	**65h00**	**61h15**	60h30	58h15	65h05	**70h35**	69h10	71h60
0.80	**69h20**	**65h20**	64h30	62h10	69h25	**75h20**	73h50	76h45
0.85	**73h40**	**69h25**	68h35	66h00	73h45	**80h00**	78h25	81h35
0.90	**78h00**	**73h30**	72h35	69h55	78h05	**84h45**	83h00	86h25
0.95	**82h20**	**77h35**	76h40	73h45	82h25	**89h25**	87h40	91h10
1.00	**86h40**	**81h40**	80h40	77h40	86h45	**94h10**	92h15	95h60
1.05	**91h00**	**85h45**	84h40	81h35	91h05	**98h50**	96h55	100h45
1.10	**95h20**	**89h50**	88h45	85h25	95h25	**103h30**	101h30	105h35
1.15	**99h40**	**93h55**	92h45	89h20	99h45	**108h15**	106h05	110h25
1.20	**104h00**	**98h00**	96h50	93h10	104h05	**112h55**	110h45	115h10
1.25	**108h20**	**102h05**	100h50	97h05	108h25	**117h40**	115h20	119h60
1.30	**112h40**	**106h15**	104h50	100h60	112h50	**122h20**	119h55	124h45

Table S2. Correspondence between experimental age and normalized age (n.a.).

---

[1] Normalized age expressed in arbitrary units, with 0 as the fertilization or activation time, and 1 as the first blastocoel collapse.

[2] Average experimental age of both WT and clones.

[3] Average experimental age of WT embryos.

[4] Average experimental age of clones.

| Normalized age	WT (3 embryos)				Clones (2 embryos)			
	Inner cells		Outer cells		Inner cells		Outer cells	
	Sym.	Asym.	Sym.	Asym.	Sym.	Asym.	Sym.	Asym.
0.75 – 0.8	1	1	9	4	3	0	8	1
0.8 – 0.85	3	3	15	6	0	0	8	2
0.85 – 0.9	3	0	17	2	4	2	16	4
0.9 – 0.95	5	4	27	2	6	1	21	1
0.95 – 1.0	6	2	41	1	5	1	20	0
1.0 – 1.05	13	5	59	1	9	0	35	1
1.05 – 1.1	6	2	36	1	5	0	13	0
Total	**37**	**17**	**204**	**17**	**32**	**4**	**121**	**9**
Average per embryo	**12.3**	**5.7**	**68**	**5.7**	**16**	**2**	**60.5**	**4.5**

Table S3. Number of symmetrical (Sym.) and asymmetrical (Asym.) divisions observed between 0.75 and 1.10 normalized age in inner and outer cells, in wild-type embryos and clones.
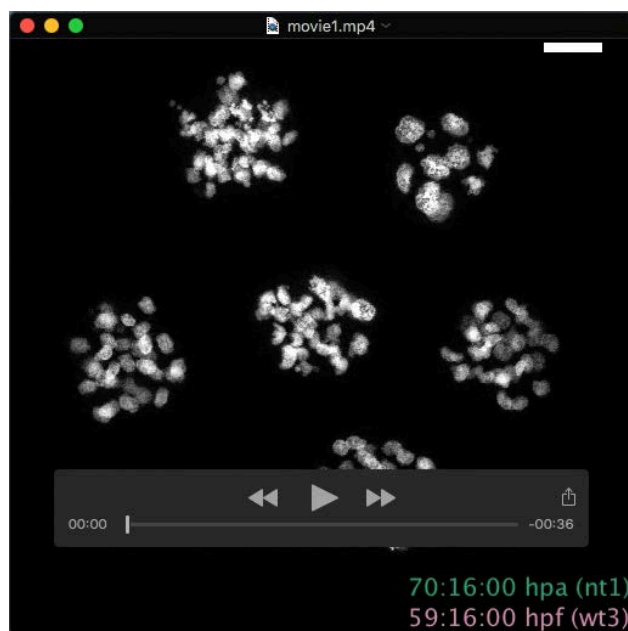
Movie S1. Imaging conditions. Development of six H2B-EGFP labeled embryos (4 wild types and 2 clones) over 50 hours under the microscope. The embryo in the middle is nt1. The top left embryo is wt3. The top right embryo is another clone, already dead before the onset of image acquisition. The three other embryos have a low signal-to-noise ratio (SNR) especially in inner cells and were not suitable for performing automated nucleus detection and tracking. The movie shows the hatching of nt1 (101.25 h.p.a.) through a small opening in its zona pellucida. The movie stops just before the hatching of wt3. Scale bar: 25 µm.
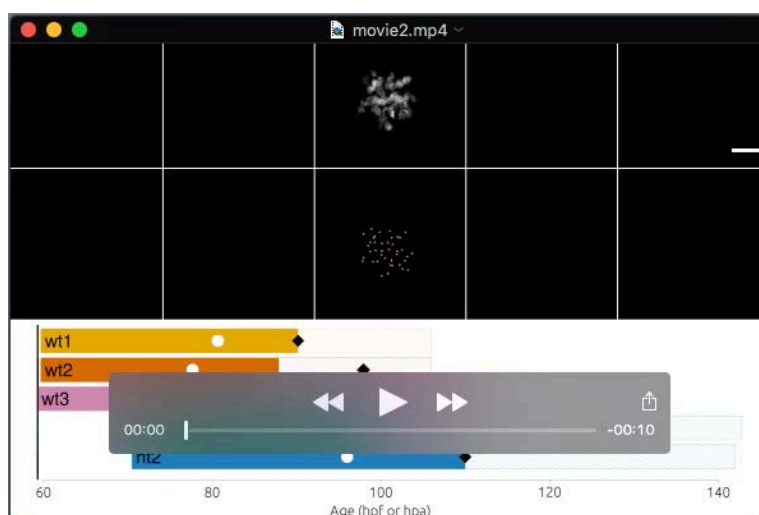

Movie S2. Raw and reconstructed data for five embryos: 3 wild types and 2 clones. Color code as in Fig. 1. (**First row**) Z-projection of 3D volumes. (**Second row**) Z-projection of reconstructed embryos synchronized with the raw data displayed in the first row. Each nucleus approximates a center and is represented by a sphere. Scale bar: 25µm for the first and second rows. (**Third row**) Timeline of the imaging sequences. The cell lineage reconstruction is limited to the colored part. White disc: first collapse. Black diamond: hatching. Age based on fertilization time (wild-type embryos) and activation time (clones).
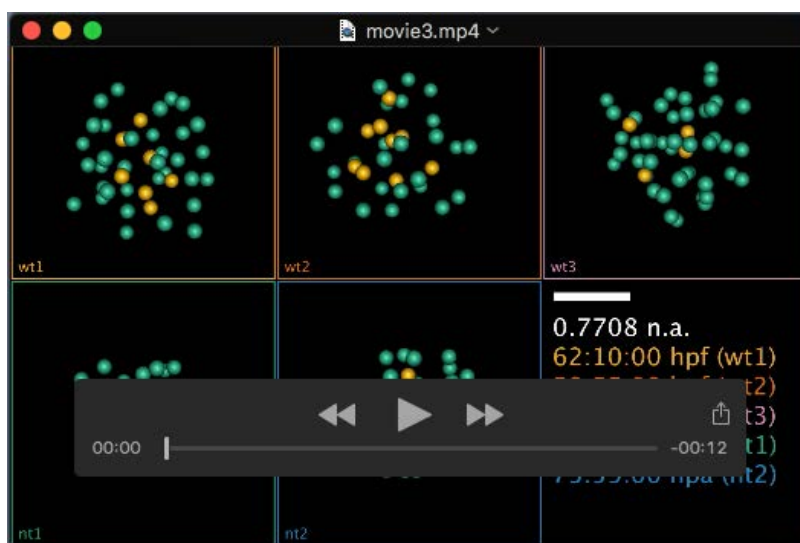
Movie S3. Inner cells and outer cells in temporally rescaled and synchronized digital specimens. Inner cells: orange spheres. Outer cells: bluish green spheres. Time is given in normalized age (n.a.) and in experimental age for the different embryos with the color code used in Fig. 1. Scale bar: 25 µm.
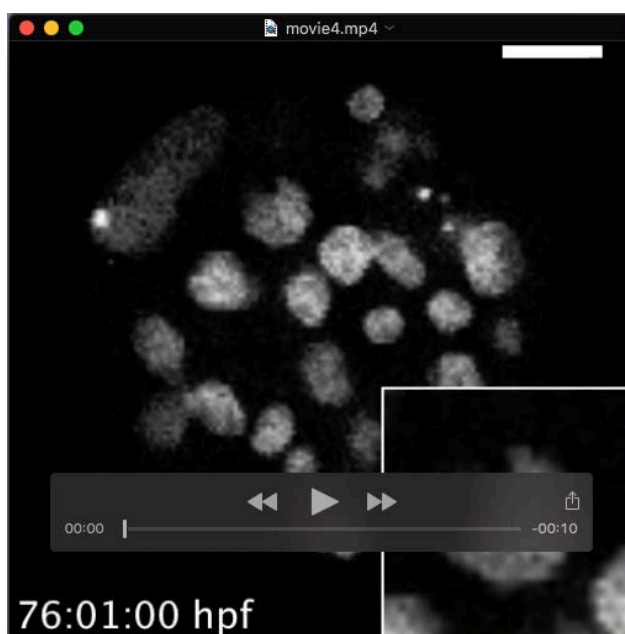
Movie S4. Cell death annotation (in wt3). Z projection of a 10.5 µm thin section (10 slices) of wt3 starting at 76 h.p.f, z-centered around a dying cell. Scale bar: 25 µm. Inset: 2x magnification of the dying cell.
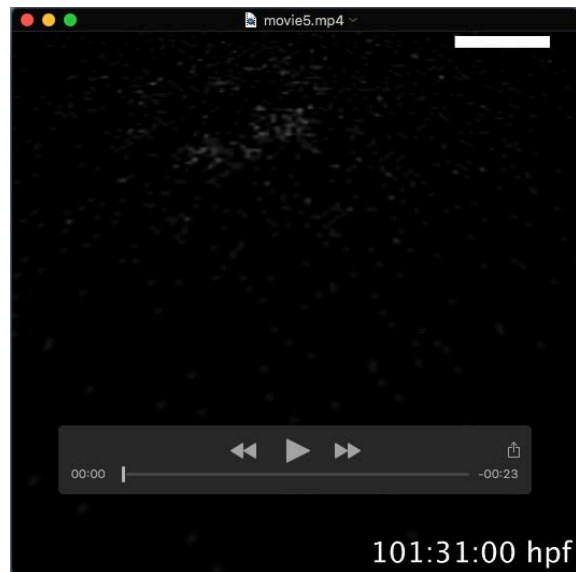
Movie S5. Asymmetric divisions in inner cell population (in wt3). An inner cell (orange) undergoes an asymmetric division and displays a prophase pattern by 101.5 h.p.f. 15 minutes later, the metaphase plate is parallel to the embryo surface. The cell of interest generates an outer daughter (bluish green, right side of the movie) and an inner daughter (orange, left side of the movie) by 102 h.p.f. 30 minutes later, the inner nucleus has reached the inner cell mass. Scale bar: 25 μm.
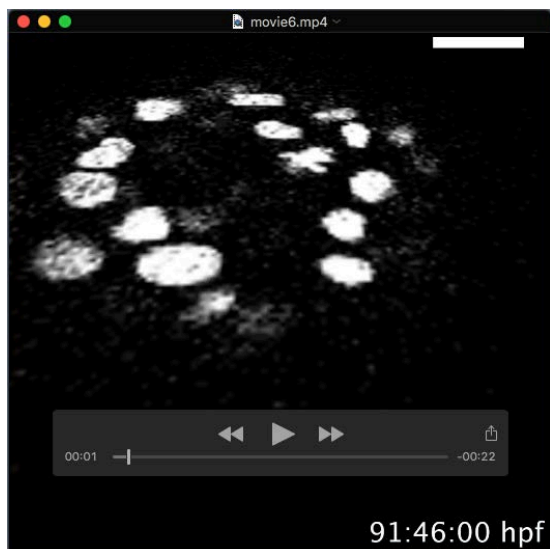
Movie S6. Asymmetric divisions in outer cell population (in wt3). An outer cell (bluish green) undergoes an asymmetric division and displays a prophase pattern by 91.75 h.p.f. 15 minutes later, the metaphase plate is parallel to the imaging plane. The mitotic cell gives rise to an outer daughter (bluish green, right side of the movie) and an inner daughter (orange, left side of the movie) by 92.25 h.p.f. 60 minutes later, the inner nucleus has reached the inner cell mass. Scale bar: 25 μm.

Note S1. Temporal rescaling based on morphogenetic events gave better results than other methods. We identified three methods to temporally rescale embryo development: 1) based on cell number only, 2) based on embryo volume only, and 3) based on morphogenetic events. As expected, the first and second methods gave very good results on the alignment of cell numbers and embryo volumes respectively. However, the variability of embryo volume was the highest after temporal rescaling with cell number, and the variability of cell number was the highest after temporal rescaling with embryo volume. Only the third method gave a good compromise between cell number alignment and embryo volume alignment, i.e., leading to similar curves.

To find the best compromise, we calculated a distance between the curves for each method and for each pair of embryos. The distance was calculated as the average of the Euclidean distance between the two curves. The distance was normalized between 0% (smallest distance, best alignment) and 100% (largest distance, worst alignment) and an average score was calculated for volume and cell number alignment. Method 1 obtained a mean score of 32% (6% for cell number alignment and 57% for volume alignment). Method 2 obtained a mean score of 34% (53% for cell number alignment and 15% for volume alignment). Method 3 obtained a mean score of 28% (26% for cell number alignment and 30% for volume alignment), and was therefore used for further embryonic comparisons.